XVI International Conference on Computational Plasticity. Fundamentals and Applications
COMPLAS 2021
E. Oñate, D. Peric, M. Chiumenti and Eduardo de Souza Neto (Eds)

LOCALIZATION OF PLASTIC DEFORMATION IN STRETCHING PLATES: MICROSTRUCTURE EFFECTS

J.L. DEQUIEDT [*,†] **AND C. DENOUAL** [*,†]

[*] CEA, DAM, DIF, F-91297 Arpajon France
e-mail: jean-lin.dequiedt@cea.fr, christophe.denoual@cea.fr

[†] Université Paris-Saclay, CEA, LMCE, F-91680 Bruyères-le-Chatel, France

Key words: Crystal Plasticity Simulation, Plastic Strain Localization, Necking, Metals, Texture.

Abstract. The incidence of microstructural characteristics on the localization of plastic deformation in stretching plates in the form of necking was investigated by performing polycrystal plasticity simulations: crystal aggregates were generated by a Voronoï tessellation algorithm and crystal orientations were randomly distributed among the grains. The most outstanding results of this analysis, detailed in [1], are presented here. During dynamic extension, a transition is displayed between an initial grain scale strain organization towards the development of much larger patterns and a final stage during which one or a few localization zones develop drastically. The influence of the initial strain distribution on the final necking framework is enhanced when the number of grains in the plate thickness is reduced or the loading rate is moderate. Additionally, the sensitivity of the different stages of the localization process to texture has been highlighted: the co-existence of both favorably and unfavorably oriented grains raises the initial strain heterogeneity and triggers macroscopic localization at shorter times.

1 INTRODUCTION

The localization of plastic deformation in dynamically expanding shells in the form of multiple necks is well documented and analyzed at the macroscopic scale as an outcome of the development of instable perturbation modes of the homogeneous response of the structure. In the aim of predicting the onset of necking, linear stability analysis (LSA) was achieved by many authors following the early works of Fressengeas and Molinari [2] and Shenoy and Freund [3]. Among others, the cases of plates under plane strain and biaxial stretching were investigated in [4] and [5,6] respectively; an extension of LSA to a time varying homogeneous solution was also proposed in [7]. In the early stages, instable modes with the highest growing rates control the spacing of areas of strain concentration. Next, these zones interact and give rise to the necking pattern, some of them being inhibited by stress release fronts emitted by the most developed ones; such a shielding process was first analyzed by Mott [8].

However, when the polycrystalline structure of the shell is considered, the deformation is inherently heterogeneous since the beginning of loading and a continuous transition arises, from grain size organization at short time, to macroscopic localization at long time. Both

initial strain pattern formation and final necking process may be influenced by physical characteristics such as grain size, texture or dislocation densities (shell microstructure is an outcome of the forming operation). In the present work, FE crystal plasticity simulations of stretching tantalum sheets mimicking expanding shells are provided. The crystal plasticity model and simulated geometry are defined in Section 2. Uniaxial stretching of an isotropic sheet is presented in Section 3 for two different strain rates and grain sizes: the interplay between grain scale response and structural modes is investigated. Section 4 is concerned with biaxial stretching for both an isotropic and a strongly textured plate: the impact of marked "fibers" on the different steps of the necking process is emphasized.

2 CRYSTAL PLASTICITY MODEL AND SIMULATED AGGREGATES

The single crystal constitutive behavior is formulated in finite deformations and a Teodosiu type model taking dislocation densities as internal state variables is retained [9]. Namely, the deformation gradient tensor decomposes into an elastic and a plastic part, the elastic transformation encompassing lattice deformations and rotations (the relaxed configuration is said "isoclinic"):

$$\mathbf{F} = \mathbf{F}^e \cdot \mathbf{F}^p. \tag{1}$$

The plastic transformation rate is ensured by the slip rates on the different slip systems of the crystal lattice:

$$\mathbf{L}^p = \dot{\mathbf{F}}^p \cdot \mathbf{F}^{p-1} = \sum_\alpha \dot{\gamma}^\alpha \mathbf{m}_0^\alpha \otimes \mathbf{n}_0^\alpha. \tag{2}$$

Tantalum is a BCC structure for which 24 slip systems are considered: 12 with {110} slip planes and 12 with {112} slip planes. For dynamic loading conditions, slip rates are provided by a thermal activation law:

$$\dot{\gamma}^\alpha = \dot{\gamma}_0 \exp\left(-\frac{\Delta G}{k_B T}\right) \qquad \text{with} \qquad \Delta G = \Delta F \left\langle \left(1 - \left(\frac{\langle \tau^\alpha - \tau_c^\alpha \rangle}{s}\right)^p\right)^q \right\rangle. \tag{3}$$

The resolved shear stress τ^α is the projection of the stress tensor on the slip system and expresses in finite deformations ($\boldsymbol{\pi}$ is the second Piola-Kirchhoff stress tensor related to the relaxed configuration):

$$\tau^\alpha = (\mathbf{F}^{eT} \cdot \mathbf{F}^e \cdot \boldsymbol{\pi}) : (\mathbf{m}_0^\alpha \otimes \mathbf{n}_0^\alpha). \tag{4}$$

Strain hardening is quantified by the evolution of the critical shear stress with dislocation densities per system:

$$\tau_c^\alpha = \tau_0 + \mu b \sqrt{\sum_\beta a^{\alpha\beta} \rho^\beta}. \tag{5}$$

The hardening matrix $a^{\alpha\beta}$ is derived from dislocation dynamics simulations and coefficients for tantalum are given in [10]. The evolution of dislocation densities is driven by the competition between dislocation storage and annihilation by dynamic recovery:

$$\dot{\rho}^\alpha = \frac{1}{b}\left(\sqrt{\sum_\beta d^{\alpha\beta} \rho^\beta} - 2 y_c \rho^\alpha\right) \dot{\gamma}^\alpha. \tag{6}$$

Sheet simulations (cf. Fig. 1) are performed with the crystal plasticity code Coddex using an Element Free Galerkin numerical scheme. A Voronoï tessellation algorithm is used to

generate both 4000 and 50000 grain aggregates: a random selection of 100 crystal orientations is distributed among these grains.

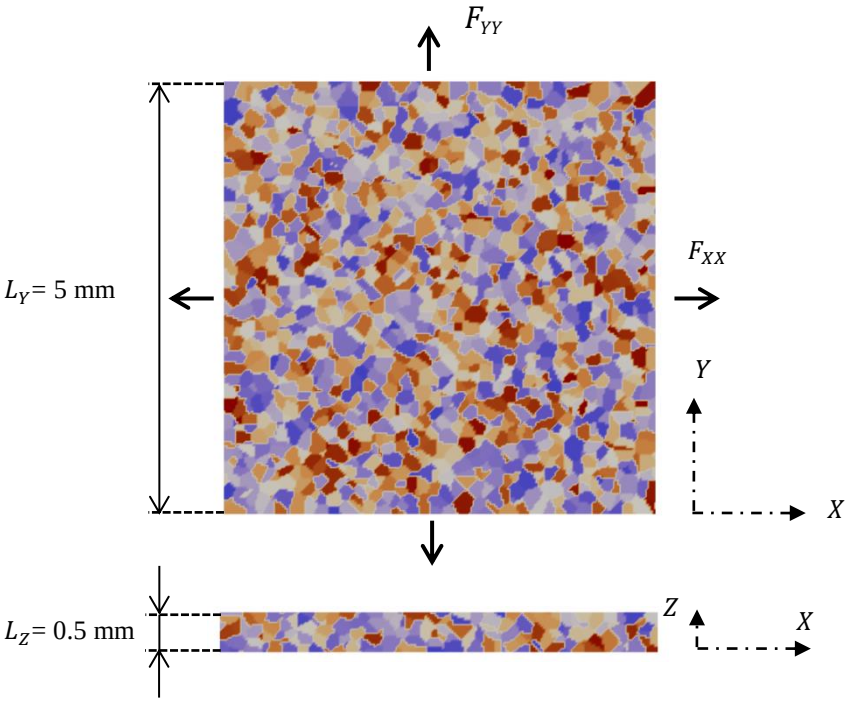

Figure 1: Simulated stretching sheet in the case of a 4000 grain aggregate.

Periodic boundary conditions and an average deformation gradient **F** ($F_{YY} = 0$) are imposed in the sheet plane, the upper and lower faces being free of loading. Both plane strain ($F_{YY} = 0$) and equi-biaxial ($F_{YY} = F_{XX}$) loadings are considered. A mesh of 200*200*20 nodes is chosen as a compromise between computational cost and resolution (for the 50000 grain structure, it amounts to an average of 16 nodes per grain).

3 NECKING IN PLANE STRAIN STRETCHING

3.1 Influence of grain size

The transition from grain scale strain organization to macroscopic localization is illustrated for the two grain numbers at moderate stretching rate ($\dot{F}_{XX}$ = 5000 s^{-1}). Maps of equivalent Hencky strain ε^{dev} in the average plane and cross section are displayed at early and late stages (Fig. 2). Namely (**I** denotes identity tensor):

$$\varepsilon^{dev} = \sqrt{\frac{2}{3}\boldsymbol{\varepsilon}^d : \boldsymbol{\varepsilon}^d} \quad \text{with} \quad \boldsymbol{\varepsilon}^d = \boldsymbol{\varepsilon} - \frac{1}{3}\mathrm{tr}(\boldsymbol{\varepsilon})\mathbf{I} \quad \text{and} \quad \boldsymbol{\varepsilon} = \frac{1}{2}\log(\mathbf{F}^T \cdot \mathbf{F}). \tag{7}$$

When the number of grains increases, the initial strain heterogeneity is reduced and macroscopic localization is delayed. For the 4000 grain aggregate, only one localization zone remains in the late stage; the final localization path in the average plane covers grains or grain clusters in which initial strain was high, showing, in some sense, a strong memory of the

initial grain scale response. For the 50000 grain aggregate at late stage, the localization band is almost aligned with the Y-axis, as would be predicted by a macroscopic stability analysis, and the memory of the initial strain pattern is much less pronounced. In the cross section, for both grain numbers, a transition emerges from a strain initially mostly oriented at 45° from the sheet plane that eventually transforms in one main neck.

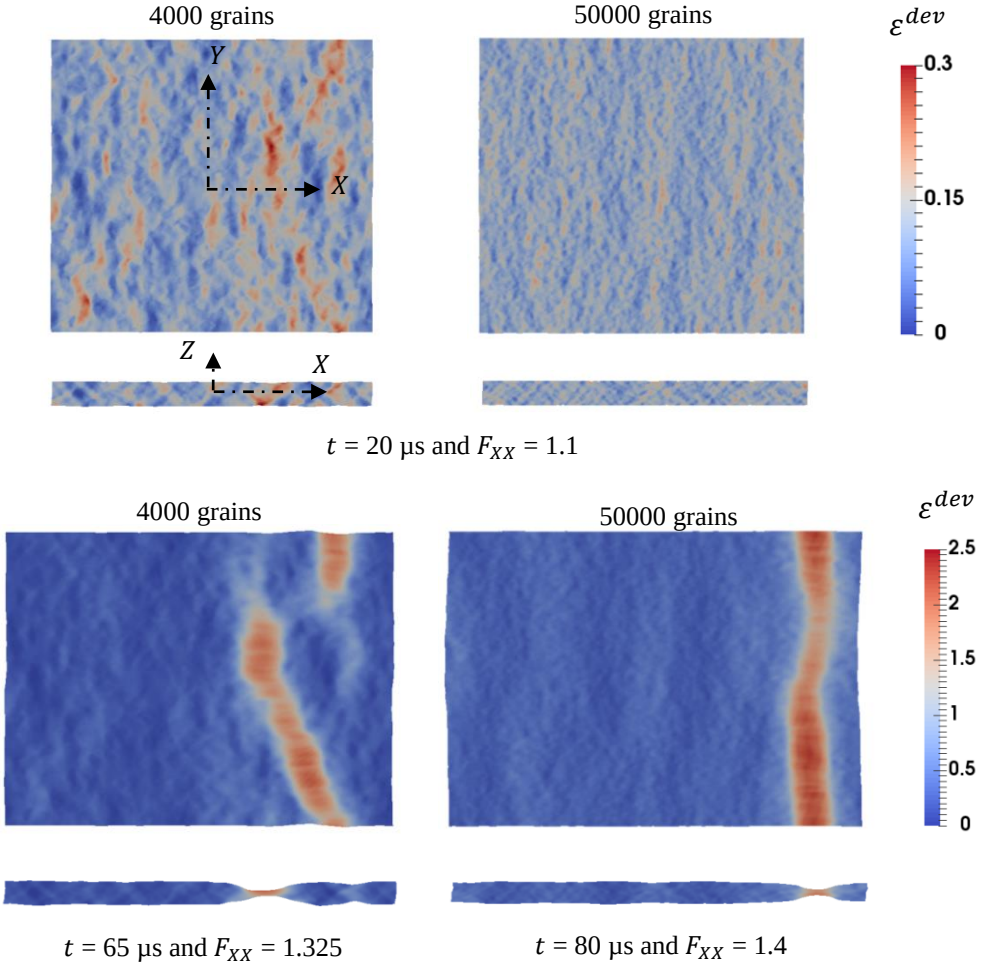

Figure 2: Maps of deviatoric (Hencky) strain ε^{dev} in average plane and cross section for the 4000 and 50000 grain aggregates for stretching rate $\dot{F}_{XX}$ = 5000 s^{-1}.

3.2 Influence of stretching rate

A more precise evaluation of the respective role of the initial grain scale strain organization, structural perturbation modes and Mott type shielding process can be achieved by comparing the two stretching rates $\dot{F}_{XX}$ = 5000 s^{-1} and $\dot{F}_{XX}$ = 25000 s^{-1} for the 50000 grain aggregate.

For $\dot{F}_{XX}$ = 25000 s^{-1}, strong localization takes place for higher mean elongation than for $\dot{F}_{XX}$ = 5000 s^{-1} and three necking bands form (Fig. 3); this result is consistent with shorter

wavelengths for dominant perturbation modes given by LSA when the mean strain rate increases. Additionally, shielding is less efficient due to release fronts having less time to propagate.

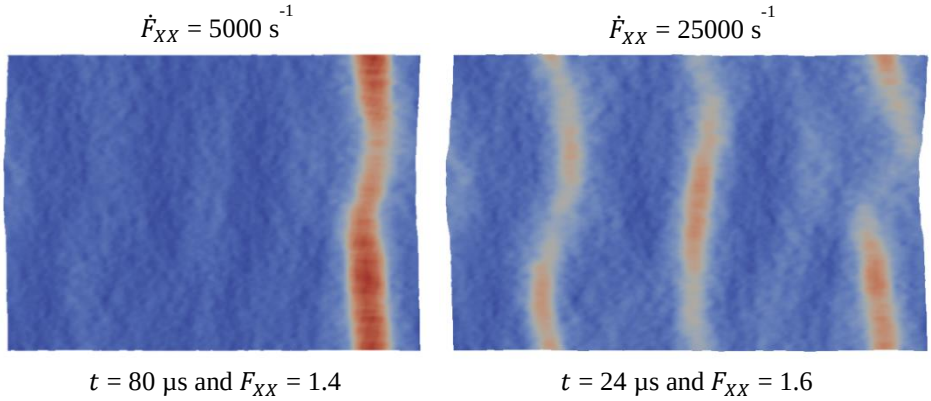

Figure 3: Maps of Hencky strain ε^{dev} in average plane for the 50000 grain aggregate and plane strain stretching in the late stage for stretching rates $\dot{F}_{XX}$ = 5000 s^{-1} and $\dot{F}_{XX}$ = 25000 s^{-1} (same color scale as Fig. 2).

A deeper insight in strain organization at the different steps of the loading process is provided by Hencky strain profiles plotted along the X-axis at different times for the two stretching rates (Fig. 4). For moderate stretching rate ($\dot{F}_{XX}$ = 5000 s^{-1}), the initial strain profile first grows keeping its shape and being slightly modulated by what could be interpreted as a structural perturbation mode. At last, one peak covering about three to four maxima of the profile bursts and seems to inhibit deformation in the rest of the structure as if a release front had shielded the whole sheet. For high stretching rate ($\dot{F}_{XX}$ = 25000 s^{-1}), delayed strong localization leaves more time for the modulation to develop and the three peaks are linked to the maxima of the modulated profile, as if structural mode controlled necking in a more conclusive way.

4 TEXTURE INFLUENCE IN BIAXIAL STRETCHING

At the grain scale, despite the level of the critical shear stresses, a measure of the resistance to plastic deformation is given by the more or less favorable orientation of the slip systems towards the loading axes; this is the reason why texture impacts plastic strain organization since the beginning of loading. This effect is quantified by the slip system Schmid factors, defined by extending the uniaxial stress formulation, $\|\mathbf{A}\|$ being the "von Mises norm" of tensor $\mathbf{A}$:

$$\eta^{\alpha} = \frac{|\tau^{\alpha}|}{\|\mathbf{F}^{eT}\cdot\mathbf{F}^{e}\cdot\boldsymbol{\pi}\|} \quad \text{with} \quad \|\mathbf{A}\| = \sqrt{\frac{3}{2}\mathbf{A}^{d} : \mathbf{A}^{d}} \quad \text{and} \quad \mathbf{A}^{d} = \mathbf{A} - \frac{1}{3}\mathrm{tr}(\mathbf{A})\mathbf{I}. \tag{8}$$

In this section, the case of an isotropic texture was compared with the one of a cross-rolling texture: the latter was approximated by computing the effect a Z-axis compression applied to each grain. It mostly consists of two "fibers", i.e. almost all crystal orientations concentrate in two sets of directions. For the minor so-called θ-fiber, direction Z is almost

aligned with one of the lattice axis (normal direction ND || {001}). For the major γ-fiber, Z is almost aligned with the diagonal to the lattice cell (ND || {111}).

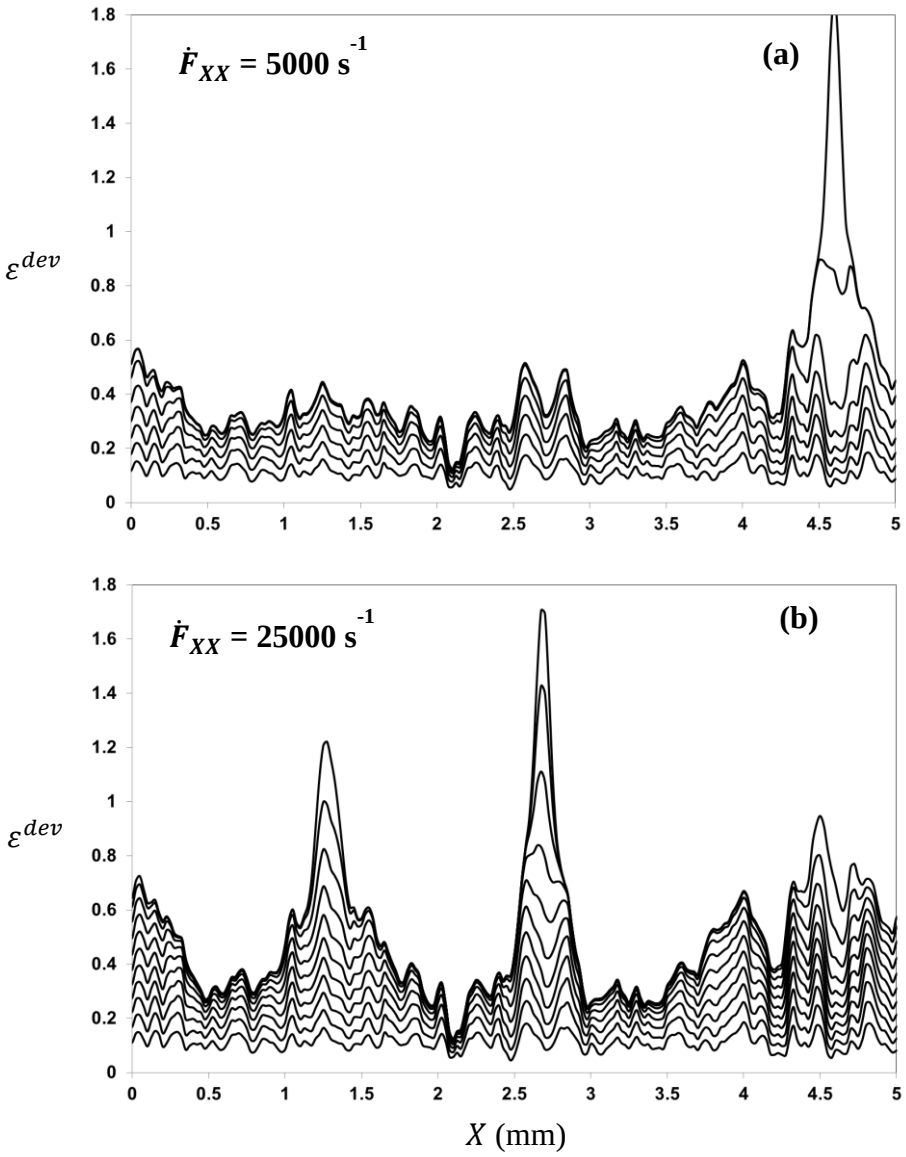

Figure 4: Strain profile for the 50000 grain aggregate on the X-axis (a) at times t = 20 μs, 40 μs, 60 μs, 80 μs and 90 μs for stretching rate $\dot{F}_{XX}$ = 5000 s^{-1} and (a) at times t = 4 μs, 8 μs, 12 μs, 16 μs, 20 μs and 24 μs for stretching rate $\dot{F}_{XX}$ = 25000 s^{-1}.

Biaxial stretching gives rise to a bi-dimensional strain organization at all stages and a final localization pattern with apparently no preferred orientation in the sheet plane. At early loading stage, strain heterogeneity is higher for the textured sheet which leads to macroscopic

localization taking place for slightly shorter times. Illustration is given in Fig. 5 for the 4000 grain sheet.

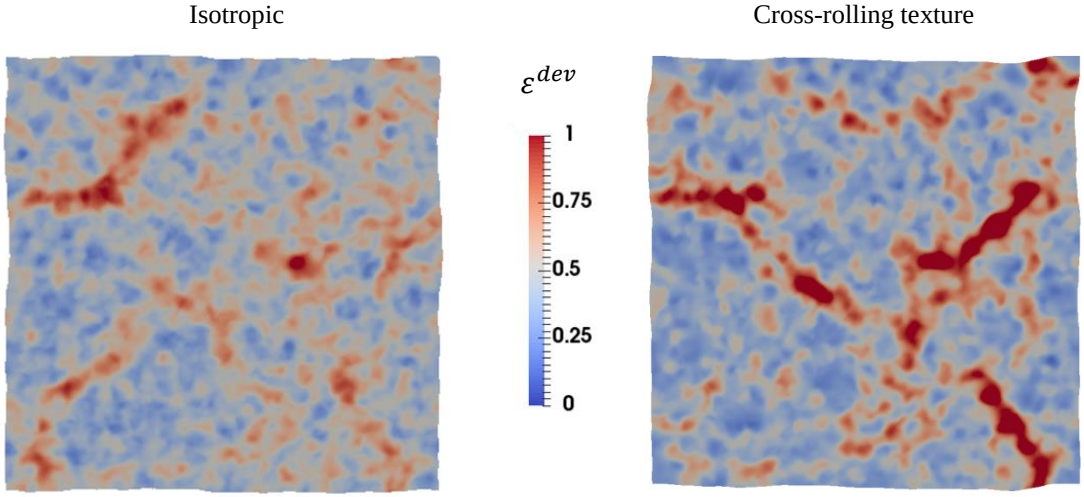

t = 80 µs and $F_{XX} = F_{YY}$ = 1.26

Figure 5: Maps of Hencky strain ε^{dev} in average plane for the 4000 grain aggregate and biaxial stretching for an isotropic and a cross-rolling texture and stretching rate $\dot{F}_{XX} = \dot{F}_{YY}$ = 3240 s^{-1}.

Cross-rolling texture: In the early stage of loading, strain is higher in the grains of the θ-fiber which is also characterized by a higher maximum Schmid factor η^{max}, as depicted on the density map of Fig. 6 for t = 20 µs. This two fiber texture remains stable up to the final stages (t = 80 µs on Fig. 6); the correlation between maximum Schmid factor η^{max} and strain ε^{dev} is however slightly weaker, probably due to the fact that necking is a structural instability mode (necks cover both favorably and unfavorably oriented grains).

Initially isotropic texture: In early stage, Schmid factors lay between about 0.3 to 0.5, ε^{dev} being higher in average for higher Schmid factors. However, Schmid factors start concentrating on two values around 0.3 and 0.5 respectively. This is a clear indication that a texture is starting to develop and one could establish that θ and γ fibers are forming. In other words, pronounced macroscopic localization is preceded by texture formation. No clear conclusion can be proposed concerning the strain vs. maximum Schmid factor correlation at the late stages.

5 CONCLUSION

Plastic strain organization in stretching metal sheets – influenced by texture, grain size and the way deformation settles at the mesoscopic scale – controls to some extent the timescale and the shape of the macroscopic localization pattern formation. According to the first results presented here, it comes that for large grains and moderate strain rate, initial strain concentrations trigger potential necking sites next interacting by a Mott type shielding process. On the contrary, for smaller grains and high strain rates, structural perturbation modes tend to overtake grain scale strain fluctuations and drive the location and spacing of the

final necks. The interplay between texture and grain scale strain organization can modify the whole process, especially when co-existence of favorably and unfavorably oriented fibers enhances strain heterogeneity.

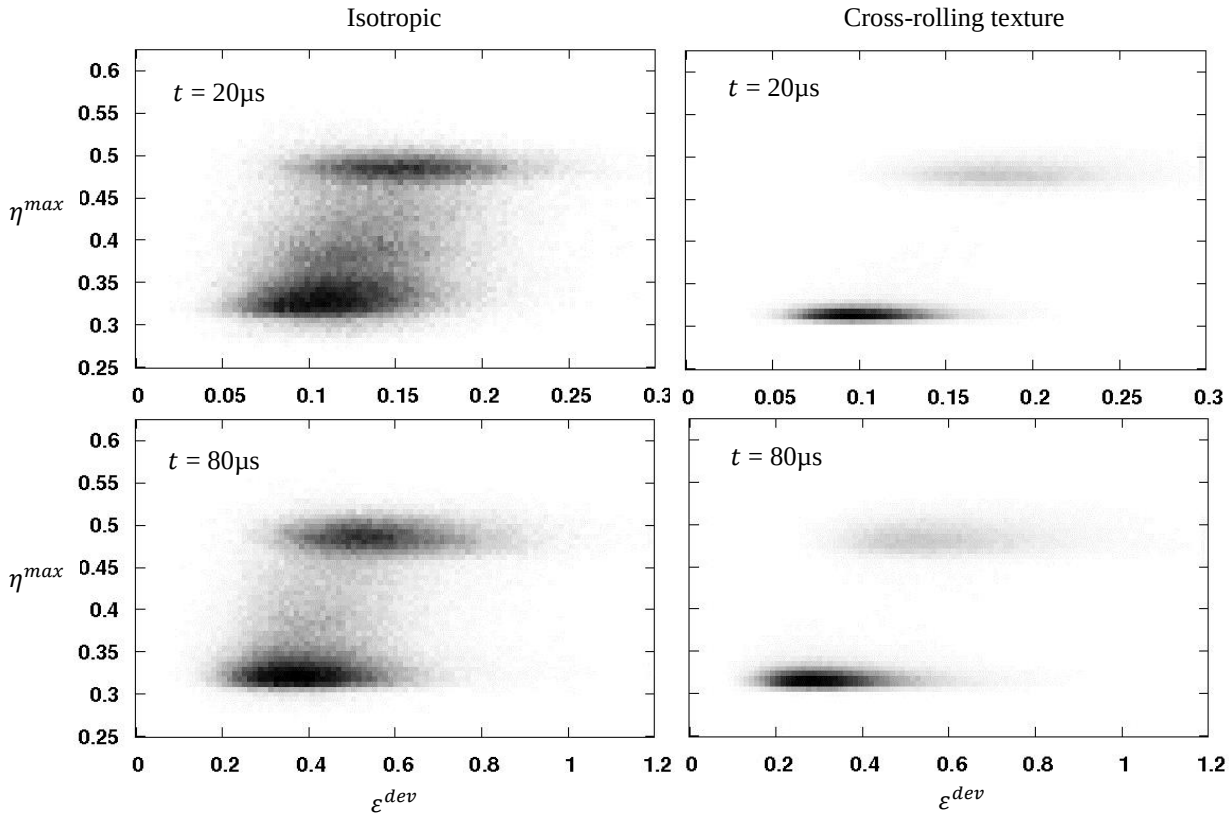

Figure 6: Density maps in a maximum Schmid factor versus strain intensity plane at different times for the 4000 grain aggregate and biaxial stretching for an isotropic and a cross-rolling texture (stretching rates are $\dot{F}_{XX} = \dot{F}_{YY}$ = 3240 s^{-1}).

REFERENCES

[1] Dequiedt, J.L., Denoual, C., Localization of plastic deformation in stretching sheets with a crystal plasticity approach: Competition between weakest link and instable mode controlled process. *Int. J. Solids Struct.* (2021), **210-211**: 183-202.

[2] Fressengeas, C., Molinari, A. Fragmentation of rapidly stretching sheets. *Eur. J. Mech. A/Solids* (1994) **13**: 251-268.

[3] Shenoy, V.B., Freund, L.B. Necking bifurcations during high strain rate extension. *J. Mech. Phys. Solids* (1999) **47**: 2209-2233.

[4] Mercier S., Molinari, A. Predictions of bifurcation and instabilities during dynamic extension. *Int. J. Solids Struct.* (2003) **40**: 1995-2016.

[5] Jouve, D. Analytic study of the onset of plastic necking instabilities during biaxial tension tests on metallic plates. *Eur. J. Mech. A/Solids* (2015) **50**: 59-69.

[6] Rodriguez-Martinez, J.A., Molinari, A., Zaera, R., Vadillo, G., Fernandez-Saez, J. The

critical neck spacing in ductile plates subjected to dynamic biaxial loading: on the interplay between loading path and inertia effects. *Int. J. Solids Struct.* (2017) **108**: 74-84.

[7] Xavier, M., Czarnota, C., Jouve, D., Mercier, S., Dequiedt, J.L., Molinari, A. Extension of linear stability analysis for the dynamic stretching of plates: spatio-temporal evolution of the perturbation. *Eur. J. Mech. A/Solids* (2020) **79**: 103860.

[8] Mott, N.F. Fragmentation in shell cases. *Proc. Roy. Soc. Ser. A* (1947) **189**: 300-308.

[9] Teodosiu, C., Raphanel, J.L., Tabourot, L. Finite element simulation of the large elastoplastic deformation. In: *Large Plastic Deformations* edited by Teodsiu C., Raphanel J.L., Sidoroff F., Rotterdam, A.A. Balkema, pp. 153-168 (1991).

[10] Madec, R., Kubin, L.P. Dislocation strengthening in FCC metals and in BCC metals at high temperatures. *Acta Mater.* (2017) **126**: 166-173.